Philippine Journal of Science
149 (3-a): 801-813, October 2020
ISSN 0031 - 7683
Date Received:13 Apr 2020

Electrochemical Reversible Copper Oxide (CuO) System on Multiwalled Carbon Nanotube Paste Electrode (CPE) as Sensor for Hydrogen Peroxide in Wound Cleaning Solution

Angelo Gabriel E. Buenaventura[1,2] and **Allan Christopher C. Yago**[1,2]*

[1]Institute of Chemistry; [2]Natural Sciences Research Institute
University of the Philippines, Diliman, Quezon City 1101 Philippines

An electrochemical sensor for hydrogen peroxide (H_2O_2) was prepared and optimized in this study. The sensor recognition element consisted of mainly copper oxide (CuO) particles electrodeposited on an anodized multiwalled carbon nanotube paste electrode (MWCPE), which is composed of multiwalled carbon nanotubes (MWCNT) and polydimethylsiloxane (PDMS). Chronoamperometry (CA) was used as the electrodeposition technique both for Cu deposition and oxidation to CuO. The layer of CuO was shown to react with H_2O_2, which lead to measurable voltammetric current at varying concentrations of H_2O_2. Different parameters were optimized as follows: Cu deposition time, Cu oxidation time, and equilibration time. Differential pulse voltammetry (DPV) was used as the main sensing technique for CuO-CPE. DPV measurements showed that the average peak current (ave. Ip) was found to be increasing linearly with increasing H_2O_2 concentration. Two H_2O_2 concentration ranges, low concentration (20 µM – 100 µM) and high concentration (400 µM – 1200 µM), were observed to have a linear correlation with ave. Ip. The limits of detection (LODs) were calculated to be equal to 11.40 µM using the low concentration range, while 13.04 µM using the high concentration range. The H_2O_2 measurements using CuO-CPE were found to be reproducible and repeatable. Real sample analysis was also performed on a wound cleaning solution (*aqua oxigenada*, 6% H_2O_2 w/w) as a sample. From the measurements, the H_2O_2 concentration of the analyte was found to be 6.16% w/w; the calculated % error was equal to 2.67%. Overall, CuO-CPE composite was shown to be an effective electrochemical sensor for H_2O_2 analysis.

Keywords: carbon paste electrode, copper(II) oxide, hydrogen peroxide

INTRODUCTION

H_2O_2 is a strong oxidizing agent and bleaching agent that has many applications in various industries (Li 1996). A large portion of the world's H_2O_2 production (approximately 60%) is used in textile and paper bleaching (Hage and Lienke 2006). In the pulp and paper industry, H_2O_2 concentration in bleaching effluents is regularly monitored as a part of the quality control parameter (Zhang *et al.* 2013). In wastewater treatment, H_2O_2 has been used to reduce biochemical oxygen demand, chemical oxygen demand, offensive odor, and foaminess for both industrial and domestic wastewater (Ksibi 2006). Aside from its industrial importance, H_2O_2 is also a biologically relevant compound as it is a common intermediate in many biochemical reactions, and its concentration is an important parameter in monitoring several bioprocesses (Ping *et al.* 2010). H_2O_2 is also the active component of

*Corresponding Author: acyago@up.edu.ph

wound cleaning solutions, which are commercially known as *aqua oxigenada*. Due to the wide application of H_2O_2, its determination is of significant importance. Standard methods for H_2O_2 determination include permanganate titration and ceric sulfate titration. However, these methods are tedious as these require preparation of indicator and titrant solutions. Also, these methods can have poor accuracy measurements depending on the perception of the analyst to the color of the end-point during titrations. A more accurate method is the peroxidase enzyme catalyzer (USP Technologies). In this method, the peroxidase enzyme is utilized to catalyze the transfer of electrons from H_2O_2 to a colorimetric indicator. However, this method can only be used on aqueous samples that are free from turbidity. Because of these limitations to the mentioned methods, several sensors for H_2O_2 determination have been developed. Several methods that have been employed for H_2O_2 detection include spectrophotometry (Matsubara *et al.* 1992), chemiluminescence (Tahirović *et al.* 2007), and electrochemistry (Chen *et al.* 2006). Electrochemistry, in particular, has received great interest among researchers developing sensors for H_2O_2 due to the high sensitivity of the resulting sensor and simplicity of both instrumentation and sensing procedure. Several efforts have been done to develop a highly sensitive electrochemical sensor for H_2O_2. These sensors usually consist of electrodes that are either surface or bulk modified. Such electrode modifiers include metal nanoparticles (Yang and Li 2018; Yin *et al.* 2011), electroactive polymers (Lin *et al.* 2011; Liu *et al.* 2018), and metal oxides (Chaisuksant *et al.* 2016; Sekar *et al.* 2018; Ping *et al.* 2010).

In this study, an electrochemical sensor for H_2O_2 was developed by modifying the surface of a CPE with CuO. The CPE that was used in this study is composed of MWCNT and PDMS (10-90 carbon-polymer weight ratio), where its composition – as well as its pretreatment – has been optimized in our separate study (Buenaventura and Yago 2018). MWCNT was used as the carbonaceous component for CPE fabrication because of its numerous advantages over other carbonaceous materials. These advantages include large surface area, high conductivity, biocompatibility, and chemical and thermal stability – making MWCNT a great material for electrochemical applications (Gooding 2005). On the other hand, PDMS was used as the binder for CPE fabrication because of its capability to absorb organic compounds in an aqueous solution (Tuduri *et al.* 2002). The resulting CPE was then modified with CuO *via* electrodeposition. CuO served as an electrochemical catalyst for the redox reaction of H_2O_2 to O_2 and H_2O. CuO has been widely used for H_2O_2 electrochemical sensors (Gao and Liu 2015; Song *et al.* 2010). The unique approach on this study is the use of a facile electrochemical method of CuO synthesis directly onto to the sensor (MWCNT-PDMS CPE) surface, as compared to other studies using more complicated methods including chemical precipitation (Zhang *et al.* 2014), hydrothermal method (Neupane *et al.* 2009), and sonochemical method (Wongpisutpaisan *et al.* 2011). The fabricated sensor in this study was tested for its applicability as H_2O_2 sensor for wound cleaning solution, and it was found to have good analytical response over a wide range of H_2O_2 concentrations.

METHODOLOGY

Reagents and Materials

Copper (II) chloride ($CuCl_2$) and potassium chloride (KCl) were purchased from Ajax Finechem, both with > 95% purity. MWCNTs were purchased from Chengdu Organic Chemicals Co. Ltd., Chinese Academy of Sciences (purity: > 95%; length 10–30 μm, ID 5–10 nm, and OD 10–20 nm). H_2O_2 and all other chemicals were purchased from Sigma-Aldrich with > 95% purity. *Aqua oxigenada* (6% H_2O_2 w/w) was purchased from a local pharmacy.

Instrumentation

Cyclic voltammetry (CV), CA, electrochemical impedance spectroscopy (EIS), and DPV measurements were performed using AUTOLAB PGSTAT 302N. The three-electrode system consisted of the fabricated CPE as the working electrode, Ag/AgCl (3.0 M $KCl_{(aq)}$) electrode as the reference electrode, and a Pt rod as the auxiliary electrode. Field emission scanning electron microscopy (FE-SEM) imaging and energy dispersive x-ray (EDX) analyses were done using Hitachi SU8230 FE-SEM.

CuO-CPE Fabrication and H_2O_2 Sensing Procedure

Figure 1 shows the scheme for sensor fabrication and H_2O_2 sensing. The MWCNT-based paste electrode was fabricated using the previously optimized procedure by our group (Buenaventura and Yago 2018). In brief, MWCNT powder was combined with 500cSt PDMS in a 10:90 carbon-polymer weight ratio (w/w) and then mechanically mixed. The fabricated CPE was then anodized by using CV in 0.2 M NaOH between –0.3 V to +1.5 V for 30 cycles at 100 mV/s.

CA was utilized as the electrodeposition technique both for Cu deposition and Cu oxidation to CuO. As shown in Figure 1, Cu particles were electrodeposited by applying -0.5 V on CPE in 20mM $CuCl_{2(aq)}$ in 0.1 M $KCl_{(aq)}$ solution. Then the resulting Cu-CPE was anodized by applying +0.7 V in 0.1 M NaOH solution. The fabricated CuO-CPE was then tested for H_2O_2 sensing.

The CuO-CPE was first dipped in a stirred solution of

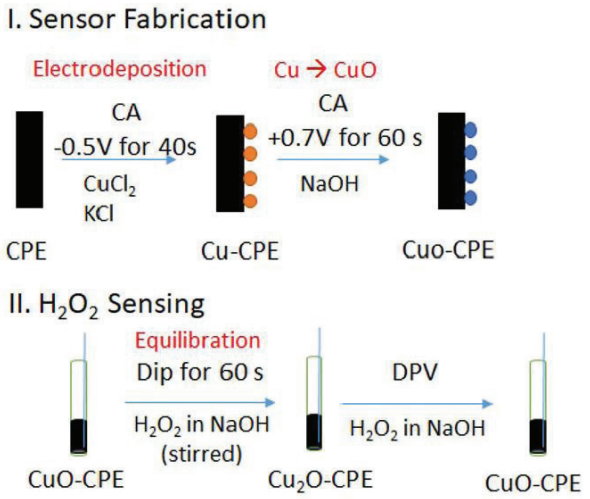

Figure 1. Scheme for sensor fabrication and H_2O_2 sensing. CA was utilized both for electrodeposition of Cu particles and oxidation of Cu to CuO. DPV was used for H_2O_2 sensing.

H_2O_2 in NaOH for equilibration for a certain period of time; then, immediately, an electrochemical measurement was done using DPV (potential range: –0.1 V to +0.8 V; scan rate: 10 mV/s; step potential: 50 mV; modulation amplitude: 25 mV; modulation time: 50 ms; interval time: 500 ms). A separate CPE was post-treated similar to the fabrication of CuO-CPE but without $CuCl_{2(aq)}$, in order to directly compare its response towards H_2O_2 with CuO-CPE. This post-treated CPE will be termed here as treated CPE.

The following parameters were optimized in this study: (1) Cu deposition time, (2) Cu oxidation time, and (3) equilibration time. Cu deposition time is defined as the amount of time the reduction potential (–0.5 V *vs.* Ag/AgCl) is applied on the CPE to deposit Cu particles on the electrode surface, producing Cu-CPE. The Cu oxidation time is defined as the amount of time the oxidation potential (+0.7 V *vs.* Ag/AgCl) is applied on the Cu-CPE to oxidize the Cu particles to CuO, thus producing CuO-CPE. Lastly, the equilibration time is defined as the amount of time the CuO-CPE is equilibrated with the sensing solution under stirring condition. CV technique was performed for the optimization of these parameters. The optimizations were based on the response of CuO-CPE towards 20 μM H_2O_2 in 0.1 M NaOH. The parameter value that gave the highest ave. Ip was chosen as the optimized value for the parameter under study.

Real sample analysis was done using *aqua oxigenada* (6% H_2O_2 w/w) as the sample. A set of NaOH solutions (0.1 M) were spiked with the sample, which was then subjected to H_2O_2 measurements using CuO-CPE. Each set of analyses (*e.g.* optimization of parameters, sensor calibration, and real sample analysis) was done within a day.

RESULTS AND DISCUSSION

Fabrication of CuO-CPE

In this study, an electrochemical sensor for H_2O_2 was fabricated by modifying the surface of CPE with CuO particles. CuO electrodeposition involves $Cu_{(s)}$ electrodeposition and $Cu_{(s)}$ oxidation. In order to achieve an efficient $Cu_{(s)}$ electrodeposition and $Cu_{(s)}$ oxidation, the potentials applied were determined and the amount of time these potentials will be applied must be optimized. In order to determine the reduction potential to be applied for $Cu_{(s)}$ deposition on the CPE surface, the electrochemical behavior of $Cu^{2+}_{(aq)}$ on CPE was first studied. Figure 2A shows the CV curve for 20 mM $Cu^{2+}_{(aq)}$ in 0.1 M $KCl_{(aq)}$ solution (pH 4.40). Several reduction and oxidation peaks

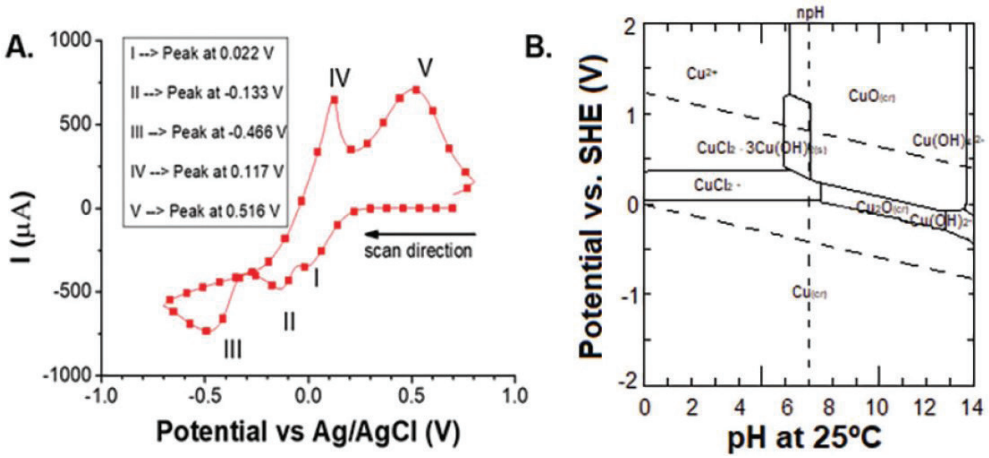

Figure 2. (A) CV curve for 20 mM $CuCl_2$ in 0.1M $KCl_{(aq)}$ using CPE; I, II, III, IV, and V are voltammetric peaks. (B) Reference Pourbaix diagram of copper-chlorine-water system; $[Cu_{(aq)}]_{total} = 10^{-4}$ molal and $[Cl_{(aq)}]_{total} = 0.2$ molal (adapted from Beverskog and Puigdomenech 1998).

can be observed, owing to multiple oxidation states of Cu. The redox couples involved in the voltammetric peaks observed can be identified using the Pourbaix diagram of copper-chlorine-water system (Figure 2B).

As seen in Figure 2A, a reduction peak at around 0.022 V (Peak I) is observed, which can be due to the reduction of $Cu^{2+}_{(aq)}$ to $CuCl_2^-{}_{(aq)}$. Another reduction peak is observed at around –0.133 V (Peak II), which can be due to the reduction of $CuCl_2^{-}{}_{(aq)}$ to $Cu_{(s)}$. Another reduction peak at around –0.466 V (Peak III) can be due to the reduction of $H^+_{(aq)}$ to $H_{2(g)}$ presented as a dashed line in the lower portion of the Pourbaix diagram. An oxidation peak is observed at around 0.117 V (Peak IV), which can be due to oxidation of $Cu_{(s)}$ to $CuCl_2^{-}{}_{(aq)}$. Lastly, an oxidation peak at around 0.516 V (Peak V) is observed, which can be due to oxidation of $CuCl_2^-{}_{(aq)}$ to $Cu^{2+}_{(aq)}$. To ensure complete reduction of $Cu^{2+}_{(aq)}$ to $Cu_{(s)}$, –0.5 V was chosen as the reduction potential.

The electrodeposition of $Cu_{(s)}$ particles on CPE was done *via* CA. Appendix Figure I shows the chronoamperogram for Cu deposition on CPE. Upon application of –0.5 V, exponential decay in reduction current is observed. A steady-state current is observed after 30 s of potential application. This shows that a steady reaction rate is achieved after 30 s of potential application.

After electrodeposition of $Cu_{(S)}$ on CPE, the resulting electrode was then subjected to anodization to oxidize $Cu_{(s)}$ to $CuO_{(s)}$. In order to determine the oxidation potential to be applied, the electrochemical behavior of Cu-CPE in $NaOH_{(aq)}$ solution must first be studied. Figure 3A shows the CV curve for $NaOH_{(aq)}$ solution using Cu-CPE. The redox couples associated with the voltammetric peaks in Figure 3A can be identified in the Pourbaix diagram for copper-water system (Figure 3B). From Figure 3, multiple oxidation and reduction peaks can be observed in the CV curve. The oxidation peak at around –0.122 V (Peak I) can be attributed to oxidation of Cu to $Cu(OH)_2^-{}_{(aq)}$. The oxidation peak at around +0.669 V (Peak II) can be attributed to oxidation of $Cu(OH)_2^-{}_{(aq)}$ to $CuO_{(s)}$. The reduction peak at around +0.563 V (Peak III) can be attributed to the reduction of $CuO_{(s)}$ to $Cu(OH)_2^-{}_{(aq)}$. Lastly, the reduction peak at around –0.619 V (Peak IV) can be attributed to the reduction of $Cu(OH)_2^-{}_{(aq)}$ back to $Cu_{(s)}$. Although the bulk concentration of $^-OH_{(aq)}$ ions leads to a pH of around pH 13, which can dissolve $CuO_{(s)}$, the pH inside the Nernst Diffusion layer is significantly lower due to lower concentration of $^-OH_{(aq)}$ ions. NaOH solution at 0.1 M concentration has been used for CuO formation in several studies (Le and Liu 2009; Shahrokhian *et al.* 2015; Yang *et al.* 2010). To ensure complete oxidation of $Cu_{(s)}$ on the CPE surface, +0.7 V was chosen to be the oxidation potential for oxidation of $Cu_{(s)}$ to $CuO_{(s)}$.

The anodization of the Cu-CPE surface was done *via* CA. Appendix Figure II shows the chronoamperogram of 0.1 M $NaOH_{(aq)}$ using Cu-CPE. From the figure, it is clearly shown that upon application of +0.7 V potential (*vs.* Ag/AgCl), a sharp decrease in current was observed and a steady current was then immediately observed. The sharp decrease in current could be due to the oxidation of a conducting surface ($Cu_{(s)}$) to a semiconducting surface ($CuO_{(s)}$).

Response of CuO-CPE Towards H_2O_2

To study the applicability of the CuO-CPE as an electrochemical sensor for H_2O_2, CV measurements were done. The treated CPE was also tested as a comparison for CuO-CPE in terms of electrochemical response towards H_2O_2. Figure 4 shows the response of CuO-CPE and treated

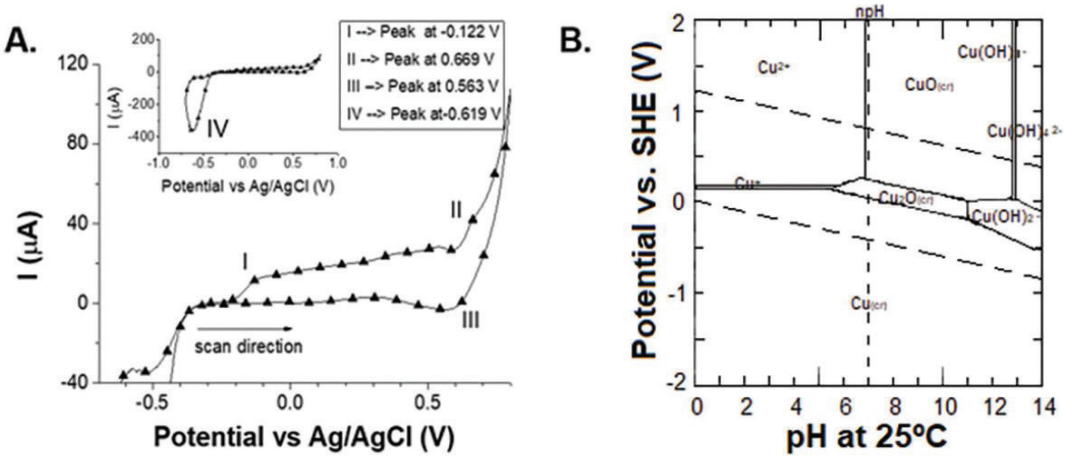

Figure 3. (A) CV curve of 0.1 M $NaOH_{(aq)}$ using Cu-CPE ($Cu_{(s)}$ deposition time: 30 s); inset shows the whole CV curve. (B) Reference Pourbaix diagram for copper-water system; $[Cu_{(aq)}]_{total} = 10^{-6}$ molal (adapted from Beverskog and Puigdomenech 1997).

$$2CuO_{(s)} + H_2O_{2(l)} \rightarrow Cu_2O_{(s)} + H_2O_{(l)} + O_{2(g)} \qquad \Delta G_{rxn} = -3.38 \text{ kJ/mol} \qquad (1)$$

$$Cu_2O_{(s)} + 3H_2O \rightarrow 2Cu(OH)_2^- + 2H^+ \qquad (2)$$

$$Cu(OH)_2^- \rightarrow CuO_{(s)} + H_2O + e^- \qquad E^\circ_{Ag/AgCl} = 0.150 \text{ V} \qquad (3)$$

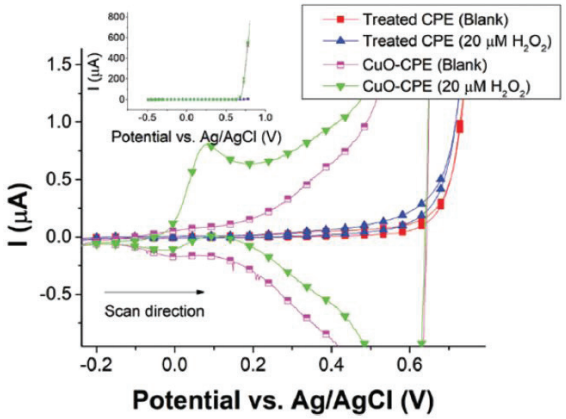

Figure 4. CV measurements of NaOH and H_2O_2 in NaOH solution using CuO-CPE (Cu deposition time: 20 s; Cu oxidation time: 60 s; equilibration time: 40 s) and treated CPE. The inset shows the whole CV curves.

CPE towards NaOH (which serves as a blank) and H_2O_2 in NaOH. CV curve using CuO-CPE showed an oxidation peak at around 0.07 V in the presence of H_2O_2. On the other hand, the CV response of treated CPE towards H_2O_2 is significantly small as compared to CuO-CPE. Furthermore, an observable increase in current in the presence of H_2O_2 is located at significantly high positive potentials (> +0.5V).

To understand the observed electrochemical behavior of CuO-CPE towards H_2O_2, it is necessary to know the reactions involved between CuO and H_2O_2. CuO can oxidize H_2O_2 to O_2 as shown in the reaction equation (Equation 1) below. This reaction is spontaneous with ΔG_{rxn} equal to –3.38 kJ/mol. Based on the Pourbaix diagram for copper-water system (Figure 3B), the formed Cu_2O is thermodynamically unstable at the solution pH, which is converted into $Cu(OH)_2^-$ upon reaction with water. The observed oxidation peak at +0.07 V using CuO-CPE can be attributed to oxidation of $Cu(OH)_2^-$ to $CuO_{(s)}$, as shown in Equation 3.

To further compare CuO-CPE and treated CPE, CV measurements were also done for H_2O_2 in NaOH solutions with different H_2O_2 concentrations using both CuO-CPE and treated CPE. Figure 5 shows CV curves of H_2O_2 solutions with different concentrations using CuO-CPE and treated CPE.

With an increasing H_2O_2 concentration, an increasing peak current at around +0.07 V can be observed using CuO-CPE. This observation further proves that the peak at +0.07 V can be associated with oxidation of $Cu(OH)_2^-$ to $CuO_{(s)}$, due to the presence of H_2O_2. On the other hand, an increasing current can be observed at significantly high potentials (> +0.5 V) using treated CPE. These significantly high potentials are not suitable for electrochemical analyses, as it would lead to significant errors in measurements in the presence of electroactive interferences.

Optimization of Different Parameters

In order to obtain the highest electrochemical response of CuO-CPE for H_2O_2, the Cu deposition time, Cu oxidation time, and equilibration time were optimized. Appendix Figure III shows the optimization of Cu deposition time. As shown in the figure, 40 s Cu deposition time showed the highest voltammetric response towards H_2O_2. Further increase in deposition time resulted in a slight decrease in its

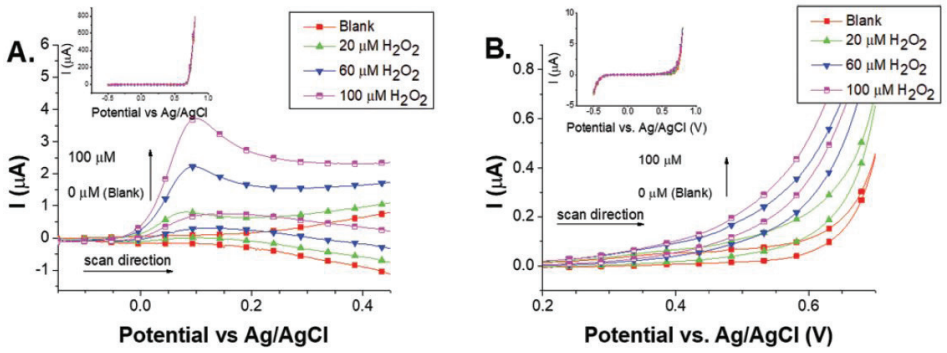

Figure 5. CV curves of 0.1M NaOH (blank) and H_2O_2 in 0.1 M NaOH solutions using (A) CuO-CPE (Cu deposition time: 20s; Cu oxidation time: 60 s; equilibration time: 40 s) and (B) treated CPE. The insets in Figures A and B show the whole CV curves.

response towards H_2O_2. This could be due to more extensive coverage of $Cu_{(s)}$ oxidized into the semiconducting CuO layer. This led to a decrease in the conductivity of the electrode surface. Therefore, 40 s was chosen to be the optimized value for the Cu deposition time.

For Cu oxidation time, 40 s deposition time was used in fabricating CuO-CPEs but with varying Cu oxidation time. Appendix Figure IV shows the optimization for Cu oxidation time. As shown in the figure, 60 s $Cu_{(s)}$ oxidation time gave the highest voltammetric response towards H_2O_2. Increasing further the oxidation time gave a similar response towards H_2O_2. A possible explanation is that the complete oxidation of $Cu_{(s)}$ to $CuO_{(s)}$ had occurred already at 60 s $Cu_{(s)}$ oxidation time. Further increase of $Cu_{(s)}$ oxidation time would not give a more oxidized area of Cu particles. From this observation, 60 s was chosen to be the optimized value for Cu oxidation time.

For equilibration time, CuO-CPEs were fabricated adopting the optimized values for $Cu_{(s)}$ deposition time (40 s) and $Cu_{(s)}$ oxidation time (60 s). Appendix Figure V shows the optimization of equilibration time for the H_2O_2 sensing procedure. As shown in the figure, an increasing trend can be observed from 10–60 s equilibration time. A possible explanation is due to increasing time for H_2O_2 molecules to react with CuO particles at the electrode surface. However, increasing further the equilibration time resulted in a significant decrease in voltammetric response, which can be due to the build-up of products of the reaction at the electrode surface. This would lead to a shift of reaction towards the reactant side, thus leading to a decrease in the voltammetric signal. With these observations, 60 s was chosen to be the optimized value for the equilibration time.

Characterization of Optimized CuO-CPE

The morphological structure of the deposited CuO on CPE was examined using FE-SEM imaging. Figure 6 shows the FE-SEM images of the CPE surface and CuO-CPE surface. The FE-SEM images were imaged using backscattered electron (BSE) mode in order to have a contrast between MWCNT-PDMS environment and CuO particles. In BSE mode, particles composed of elements with high atomic weight will appear to be brighter than its surroundings. As shown in Figure 6A, the homogenous distribution of MWCNT on the CPE surface can be observed. This is similar to the observed FE-SEM image of non-oxidized MWCNT-PDMS CPE (Buenaventura *et al.* 2016). From Figure 6B, irregularly shaped particles – which appeared to be brighter, from the surrounding environment – were suspected to be the electrodeposited $CuO_{(s)}$ particles. Aggregated $CuO_{(s)}$ particles were found in the FE-SEM image of CuO-CPE, as shown in Figure 6B. In order to prove that these particles are the electrodeposited $CuO_{(s)}$, EDX analysis was done on both CPE and CuO-CPE. Appendix Figure VI shows the EDX spectrum for both CPE and CuO-CPE. The EDX spectrum for CPE showed no peaks for the Cu element. On the other hand, the EDX spectrum for CuO-CPE showed peaks for the Cu element. These observations, thereby, prove the success of $CuO_{(s)}$ deposition on the CPE surface.

Aside from surface morphological characterization, electrochemical characterization of optimized CuO-CPE was also done. EIS measurements were obtained to evaluate the electron transfer kinetics involve using optimized CuO-CPE. Appendix Figure VII shows the Nyquist plots from EIS measurements, as well as fitted equivalent circuit models. As shown in Appendix Figure VII, CuO-CPE on NaOH alone was observed to have a highly linear Nyquist plot which could be due to impedance caused by diffusion (modeled as Warburg diffusion). This could be due to the equilibrium reaction of CuO with H_2O to form $Cu(OH)_3^-$, as represented by the vertical line in the Pourbaix diagram (Figure 3B) at around pH 13. The reaction is shown in the chemical equation below:

$$CuO + 2H_2O \rightarrow Cu(OH)_3^- + H^+ \qquad (4)$$

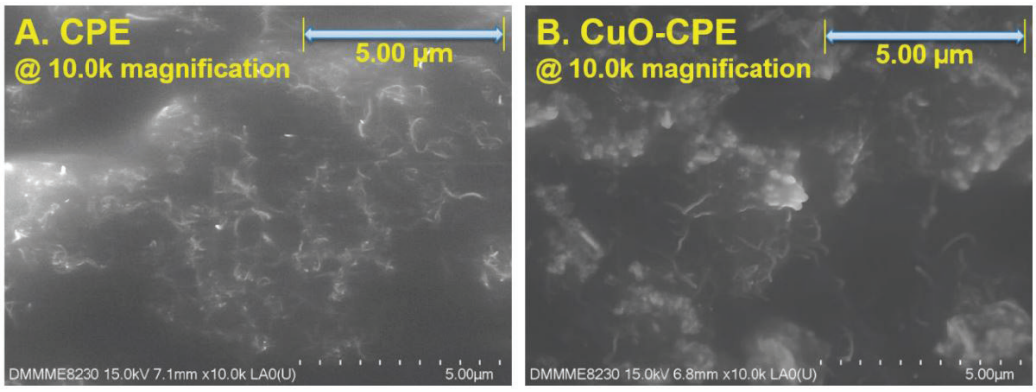

Figure 6. FE-SEM images using BSE mode of (A) CPE surface and (B) CuO-CPE ($Cu_{(s)}$ deposition time: 40 s; $Cu_{(s)}$ oxidation time: 60 s) at 10.00k magnification.

The above reaction happens beneath the electrical double layer or the capacitive layer of the electrode solution interface. Thus, the best fitted equivalent circuit is the Warburg impedance element in a series fashion with constant phase element. For H_2O_2 in NaOH solution, the Nyquist plots using CuO-CPE can be fitted with electrochemical circle fit. On the other hand, the EIS measurement of H_2O_2 in NaOH solution using CuO-CPE can be modeled with simple Randles' circuit, with the appearance of charge transfer resistance (R_{ct}) element (or polarization resistance, R_p). The R_{ct} or R_p in circuit models indicates the presence of barrier or hindrance to electron transfer at the electrode-solution interface. For the H_2O_2 solution using the CuO-CPE system, the R_p may correspond to the oxidation of $Cu(OH)_2^-$ to CuO (Equation 3), of which the conversion to the semiconducting CuO acts as a barrier to electron transfer.

H_2O_2 Determination Using CuO-CPE

For the determination of H_2O_2, DPV measurements were done using the optimized CuO-CPE. Two calibration curves were made, one for a low H_2O_2 concentration range (20 μM – 100 μM) and another one for a high H_2O_2 concentration range (200 μM – 1200 μM). Figure 7 shows the calibration curves for the two concentration ranges and their corresponding DPV curves.

As shown in Figure 7, both concentration ranges showed a linear correlation between H_2O_2 concentration and ave. Ip. The CuO-CPE thus responded linearly towards H_2O_2 concentration at both concentration ranges. To further assess the sensing performance of CuO-CPE, different figures of merit for H_2O_2 sensing were determined. Table 1 shows the determined values for different figures of merit. As shown in Table 1, the CuO-CPE has higher sensitivity at a lower concentration, thus resulting to a lower LOD and limit of quantitation (LOQ) using the lower concentration range. In terms of linearity, both of them have R-squared value close to unity, which means a linear fit is suitable for the calibration curves for both concentration ranges.

The fabrication reproducibility of the CuO-CPE sensor was also evaluated in this study. Figure 8 shows the

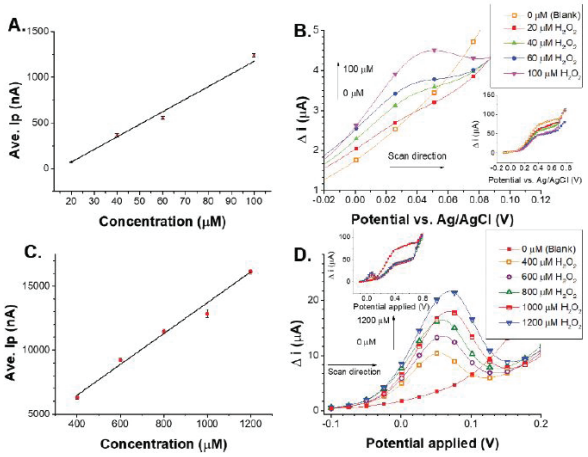

Figure 7. Calibration curves (A and C) and DPV curves (B and D) for low concentration range and high concentration range, respectively. Three measurements (n = 3) were done for each concentration. Insets in Figure B and D show the whole DPV curves.

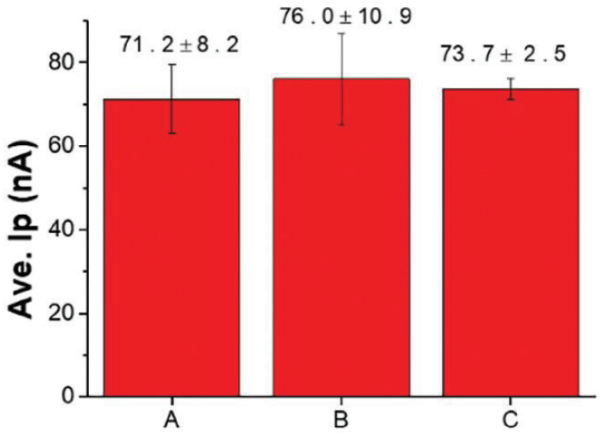

Figure 8. Ave. Ip from DPV measurements of 20 μM H_2O_2 in 0.1 M NaOH using three separate CuO-CPEs.

Table 1. Figures of merit for H_2O_2 determination using CuO-CPE.

Figures of merit	Values (for low concentration range)	Values (for high concentration range)
Linear range (μM)	20–100	400–1200
Sensitivity (nA/μM)	13.76	12.03
R-squared value	0.9925	0.9925
LOD (μM)	11.40	13.04
LOQ (μM)	37.99	43.45

*LODs and LOQs were calculated using the equations: LOD = 3 $SD_{(Blank)}$ / m and LOQ = 10 $SD_{(Blank)}$ / m. The standard error of m is equal to 0.84377 and 0.66851 for low concentration range and high concentration range, respectively.

Table 2. Peak height values from DPV measurements of 20 μM H_2O_2 in 0.1 M NaOH using CuO-CPE.

Trial	Ip (nA)
1	76.6
2	76.1
3	72.6
4	81.9
5	76.6
Ave. Ip	76.8
SD (n = 5)	3.348
% RSD	4.36

fabrication reproducibility graph for CuO-CPEs. As shown in the figure, the average responses of three separate CuO-CPEs towards H_2O_2 in NaOH did not vary significantly from each other. This is confirmed by using a single factor – analysis of variance (ANOVA), with $f_{calculated}$ (0.2718) less than $f_{critical}$ (5.1432). Thus, the fabrication of CuO-CPE can be said to be reproducible.

The reusability of CuO-CPE for H_2O_2 sensing was also evaluated in this study. Table 2 shows the peak height values from five DPV measurements of H_2O_2 in NaOH using CuO-CPE. The ave. Ip was measured to be equal to 76.8 nA with 4.36% RSD. With these measured values, the CuO-CPE can be said to be reusable over five measurements.

Real sample analysis was performed using a wound solution cleaner (6% H_2O_2 w/w) as the sample. DPV measurements showed that the average H_2O_2 concentration of the sample used is 6.16% w/w. As compared to the reported value, the measured value has a 2.67% error.

Interference study was conducted in order to assess the effect of some interferences in the H_2O_2 measurement using CuO-CPE. Two interference species were included in this study: urea and sodium phosphate. Figure 9A shows the interference study for CuO-CPE. The presence of interference (10-fold larger in concentration as compared to H_2O_2 concentration) in the sensing solution caused a larger spread in H_2O_2 measurement. The increase of spread in the measurements could be due to their interaction with the electrical double layer on the solution-electrode interface. Both urea and phosphate ion can cause a change in the size of the electrical double layer, leading to a change in non-faradaic current – a contributor to the noise of a voltammetric signal. Using ANOVA, the average values of the measurements have shown to have no significant difference with each other, where $f_{calculated}$ (0.3084) is less than $f_{critical}$ (5.1432).

Comparison with Other Studies

Due to wide applications of H_2O_2, the determination of H_2O_2 has become increasingly significant. Several groups have conducted studies that focused on sensor development for H_2O_2. Table 3 shows a list of some of the reported electrochemical sensors for H_2O_2. From the table, the CuO-CPE can be used to determine H_2O_2 at wide concentration ranges. Having a wide concentration range is important in minimizing the sample preparation procedure. More importantly – despite the simplicity of the electrode modifier – the CuO-CPE was still observed to have a low detection limit, which is only a decade higher than some of the reported electrochemical sensors with

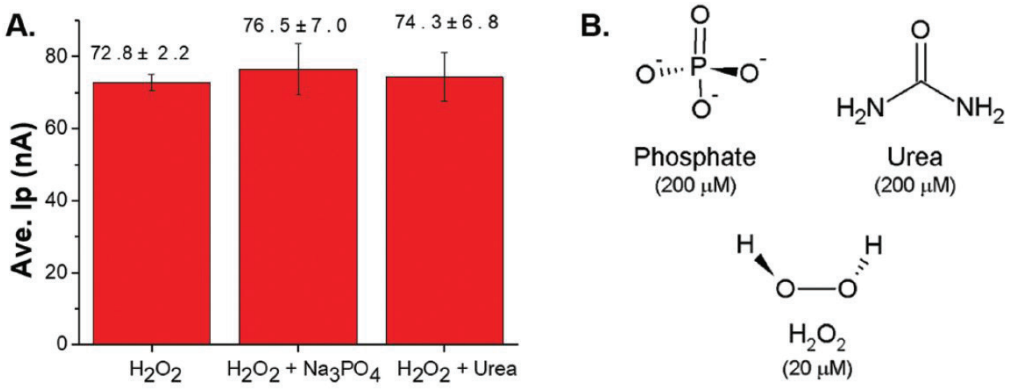

Figure 9. Interference study using CuO-CPE for H_2O_2 determination (A). Chemical structures of phosphate ion, urea, and H_2O_2 (B).

Table 3. Different studies reporting sensor for H_2O_2

Sensor	Linear range	LOD (μM)	Reference
Polypyrrole-Pt modified GCE	500 μM – 6.3 mM	0.6	Xing *et al.* 2015
MnO_2 / Au modified GCE	5.0 μM – 10 mM	1.0	Yang and Hu 2010
RGO / ZnO modified GCE	0.02 μM – 22.48 μM	0.02	Palanisamy *et al.* 2012
Au/graphene /HRP/CS modified GCE	5.0 μM – 5.13 mM	1.7	Zhou *et al.* 2010
Polypyrrole nanowire – Cu modified Au electrode	7.0 μM – 4.3 mM	2.3	Zhang *et al.* 2008
CuO-CPE	20 μM – 100 μM and 400 μM – 1.2 mM	11.4	This work

sophisticated electrode modifiers. In addition, since CuO-CPE is a modified CPE, the CuO-CPE possesses inherent advantages of CPEs over solid metallic electrodes, such as renewable surface and low-cost fabrication.

CONCLUSION

An electrochemical sensor for H_2O_2 was successfully developed in this study. FE-SEM and EDX results revealed successful electrodeposition of CuO on the CPE surface. The CuO-CPE was shown to have a significantly larger electrochemical response towards H_2O_2 as compared to a treated CPE. H_2O_2 measurements using CuO-CPE showed to be both repeatable and reproducible. Real sample analysis was successfully done using *agua oxigenada* (6% H_2O_2 w/w) as the sample with only a 2.67% error.

ACKNOWLEDGMENTS

This study was funded by the Natural Sciences Research Institute of the University of the Philippines Diliman [CHE-17-1-01], and the Philippine Department of Science and Technology.

NOTE ON APPENDICES

The complete appendices section of the study is accessible at http://philjournsci.dost.gov.ph

REFERENCES

BEVERSKOG B, PUIGDOMENECH I. 1997. Revised Pourbaix Diagrams for Copper at 25 to 300 °C. Journal of The Electrochemical Society 144(10): 3476–3483.

BEVERSKOG B, PUIGDOMENECH I. 1998. Pourbaix diagrams for the system copper-chlorine at 5–100 °C. Swedish Nuclear Power Inspectorate (SKI) Report.

BUENAVENTURA AG, LOPEZ R, YAGO AC. 2016. Carbon Nanotube – Polydimethylsiloxane Paste Electrodes as Voltammetric Sensor for Ascorbic Acid. Presented in 16th International Meeting on Chemical Sensors (IMCS 2016).

BUENAVENTURA AGE, YAGO ACC. 2018. Facile electrochemical pretreatment of multiwalled carbon nanotube – polydimethylsiloxane paste electrode for enhanced detection of dopamine and uric acid. AIP Conference Proceedings, 1958(1), 020029. doi:10.1063/1.5034560

CHAISUKSANT R, CHOMSOOK T, MANTHONG N, KALCHER K. 2016. Low Cost Hydrogen Peroxide Sensor from Manganese Oxides Modified Pencil Graphite Electrode. Procedia Chemistry 20: 81–84. doi:https://doi.org/10.1016/j.proche.2016.07.013

CHEN S, YUAN R, CHAI Y, XU L, WANG N, LI X, ZHANG L. 2006. Amperometric Hydrogen Peroxide Biosensor Based on the Immobilization of Horseradish Peroxidase (HRP) on the Layer-by-Layer Assembly Films of Gold Colloidal Nanoparticles and Toluidine Blue. Electroanalysis 18(5): 471–477. doi:10.1002/elan.200503424

GAO P, LIU D. 2015. Facile synthesis of copper oxide nanostructures and their application in non-enzymatic hydrogen peroxide sensing. Sensors and Actuators B: Chemical 208: 346–354. doi:https://doi.org/10.1016/j.snb.2014.11.051

GOODING JJ. 2005. Nanostructuring electrodes with carbon nanotubes: a review on electrochemistry and applications for sensing. Electrochimica Acta 50(15): 3049–3060. doi:http://dx.doi.org/10.1016/j.electacta.2004.08.052

HAGE R, LIENKE A. 2006. Applications of Transition-Metal Catalysts to Textile and Wood-Pulp Bleaching. Angewandte Chemie International Edition 45(2): 206–222. doi:10.1002/anie.200500525

KSIBI M. 2006. Chemical oxidation with hydrogen peroxide for domestic wastewater treatment. Chemical Engineering Journal 119(2): 161–165. doi:https://doi.org/10.1016/j.cej.2006.03.022

LE W-Z, LIU Y-Q. 2009. Preparation of nano-copper oxide modified glassy carbon electrode by a novel film plating/potential cycling method and its characterization. Sensors and Actuators B: Chemical 141(1): 147–153. doi: https://doi.org/10.1016/j.snb.2009.05.037

LI Y. 1996. Biological properties of peroxide-containing tooth whiteners. Food and Chemical Toxicology 34(9): 887–904. doi:https://doi.org/10.1016/S0278-6915(96)00044-0

LIN M, YANG J, CHO M, LEE Y. 2011. Hydrogen peroxide detection using a polypyrrole/Prussian blue nanowire modified electrode. Macromolecular Research 19(7): 673–678. doi:10.1007/s13233-011-0707-1

LIU F, AN B, ZHANG J, NIU S, WAN J. 2018. Electrochemical determination of hydrogen peroxide using a novel Prussian blue – polythiophene – graphene oxide membrane-modified glassy carbon electrode. Instrumentation Science & Technology 46(2): 207–221. doi:10.1080/10739149.2017.1376284

MATSUBARA C, KAWAMOTO N, TAKAMURA K. 1992. Oxo[5,10,15,20-tetra(4-pyridyl)porphyrinato] titanium(IV): an ultra-high sensitivity spectrophotometric reagent for hydrogen peroxide. Analyst 117(11): 1781–1784. doi:10.1039/AN9921701781

NEUPANE MP, KIM Y-K, PARK I-S, KIM K-A, LEE M-H, BAE T-S. 2009. Temperature driven morphological changes of hydrothermally prepared copper oxide nanoparticles. Surface and Interface Analysis 41(3): 259–263. doi:10.1002/sia.3009

PALANISAMY S, CHEN S-M, SARAWATHI R. 2012. A novel nonenzymatic hydrogen peroxide sensor based on reduced graphene oxide/ZnO composite modified electrode. Sensors and Actuators B: Chemical. p. 166–167, 372–377. doi:https://doi.org/10.1016/j.snb.2012.02.075

PING J, RU S, FAN K, WU J, YING Y. 2010. Copper oxide nanoparticles and ionic liquid modified carbon electrode for the non-enzymatic electrochemical sensing of hydrogen peroxide. Microchimica Acta 171(1): 117–123. doi:10.1007/s00604-010-0420-3

SEKAR NK, BHARGAVI M, PRABAKARAN L, NESAKUMAR N, SHANKAR P, KARANAM J, KRISHNAN UM, RAYAPPAN JBB. 2018. Fabrication of Electrochemical Biosensor with ZnO-PVA Nanocomposite Interface for the Detection of Hydrogen Peroxide (Vol. 17).

SHAHROKHIAN S, KOHANSAL R, GHALKHANI M, AMINI MK. 2015. Electrodeposition of Copper Oxide Nanoparticles on Precasted Carbon Nanoparticles Film for Electrochemical Investigation of anti-HIV Drug Nevirapine. Electroanalysis 27(8): 1989–1997. doi:10.1002/elan.201500027

SONG M-J, HWANG SW, WHANG D. 2010. Non-enzymatic electrochemical CuO nanoflowers sensor for hydrogen peroxide detection. Talanta 80(5): 1648–1652. doi:https://doi.org/10.1016/j.talanta.2009.09.061

TAHIROVIĆ A, ČOPRA A, OMANOVIĆ-MIKLIČANIN E, KALCHER K. 2007. A chemiluminescence sensor for the determination of hydrogen peroxide. Talanta 72(4): 1378–1385. doi:https://doi.org/10.1016/j.talanta.2007.01.072

TUDURI L, DESAUZIERS V, FANLO JL. 2002. Dynamic versus static sampling for the quantitative analysis of volatile organic compounds in air with polydimethylsiloxane-carboxen solid-phase microextraction fibers. Journal of Chromatography A 963(1): 49–56. doi:https://doi.org/10.1016/S0021-9673(02)00222-4

USP TECHNOLOGIES. n/d. Peroxidase Enzyme Catalyzer. Retrieved from http://www.h2o2.com/technical-library/analytical-methods/default.aspx?pid=73&name=Peroxidase-Enzyme

WONGPISUTPAISAN N, CHAROONSUK P, VITTAYAKORN N, PECHARAPA W. 2011. Sonochemical Synthesis and Characterization of Copper Oxide Nanoparticles. Energy Procedia 9: 404–409. doi:https://doi.org/10.1016/j.egypro.2011.09.044

XING L, RONG Q, MA Z. 2015. Non-enzymatic electrochemical sensing of hydrogen peroxide based on polypyrrole/platinum nanocomposites. Sensors and Actuators B: Chemical 221: 242–247. doi:https://doi.org/10.1016/j.snb.2015.06.078

YANG J, JIANG L-C, ZHANG W-D, GUNASEKARAN S. 2010. A highly sensitive non-enzymatic glucose sensor based on a simple two-step electrodeposition of cupric oxide (CuO) nanoparticles onto multi-walled carbon nanotube arrays. Talanta 82(1): 25–33. doi:https://doi.org/10.1016/j.talanta.2010.03.047

YANG YJ, HU S. 2010. Electrodeposited MnO2/Au composite film with improved electrocatalytic activity for oxidation of glucose and hydrogen peroxide. Electrochimica Acta 55(10): 3471–3476. doi:https://doi.org/10.1016/j.electacta.2010.01.095

YANG YJ, LI W. 2018. Gold nanoparticles/graphene oxide composite for electrochemical sensing of hydroxylamine and hydrogen peroxide. Fullerenes, Nanotubes and Carbon Nanostructures 26(4): 195–204. doi:10.1080/1536383X.2018.1424711

YIN J, QI X, YANG L, HAO G, LI J, ZHONG J. 2011. A hydrogen peroxide electrochemical sensor based on silver nanoparticles decorated silicon nanowire arrays. Electrochimica Acta 56(11): 3884–3889. doi:https://doi.org/10.1016/j.electacta.2011.02.033

ZHANG Q, FU S, LI H, LIU Y. 2013. A Novel Method for the Determination of Hydrogen Peroxide in Bleaching Effluents by Spectroscopy. BioResources 8(3).

ZHANG T, YUAN R, CHAI Y, LI W, LING S. 2008. A Novel Nonenzymatic Hydrogen Peroxide Sensor Based on a Polypyrrole Nanowire-Copper Nanocomposite Modified Gold Electrode. Sensors 8(8). doi:10.3390/s8085141

ZHANG Q, ZHANG K, XU D, YANG G, HUANG H, NIE F, LIU C, YANG S. 2014. CuO nanostructures: Synthesis, characterization, growth mechanisms, fundamental properties, and applications. Progress in Materials Science 60: 208–337. doi:https://doi.org/10.1016/j.pmatsci.2013.09.003

ZHOU K, ZHU Y, YANG X, LUO J, LI C, LUAN S. 2010. A novel hydrogen peroxide biosensor based on Au-graphene-HRP-chitosan biocomposites. Electrochimica Acta 55(9): 3055–3060. doi:https://doi.org/10.1016/j.electacta.2010.01.035

APPENDICES

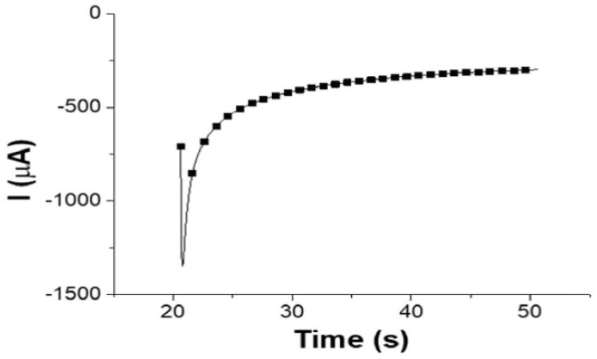

Figure I. Chronoamperogram of 20 mM $CuCl_{2(aq)}$ in 0.1 M $KCl_{(aq)}$ using CPE.
Potential applied at –0.5 V for 30 s.

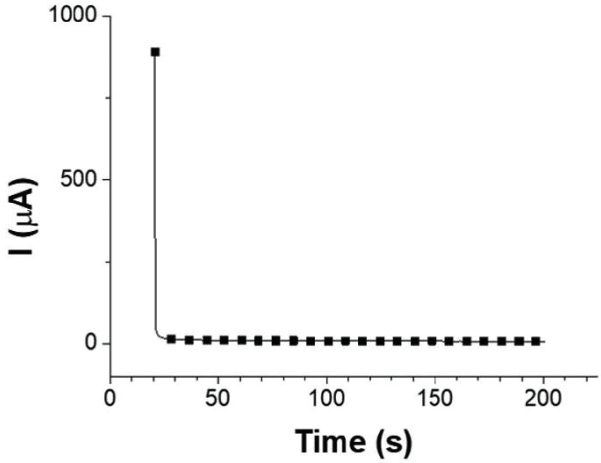

Figure II. Chronoamperogram of 0.1 M NaOH using Cu-CPE.
Potential applied: +0.7 V for 180 s.

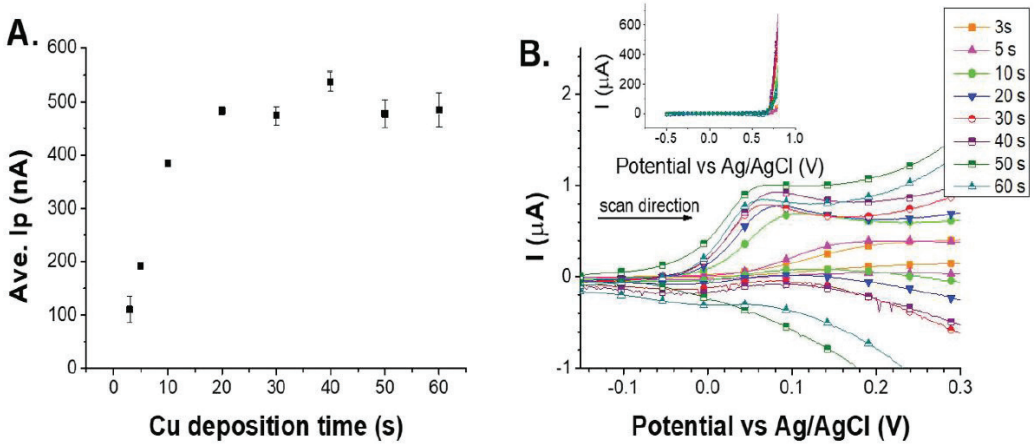

Figure III. (A) Optimization graph for the optimization of Cu deposition time. (B) CV curves of 20 μM H_2O_2 in 0.1 M NaOH using CuO-CPEs (Cu oxidation time: 60 s, equilibration time: 40 s) with different Cu deposition times; scan rate: 10 mV/s. The inset shows the whole CV curves.

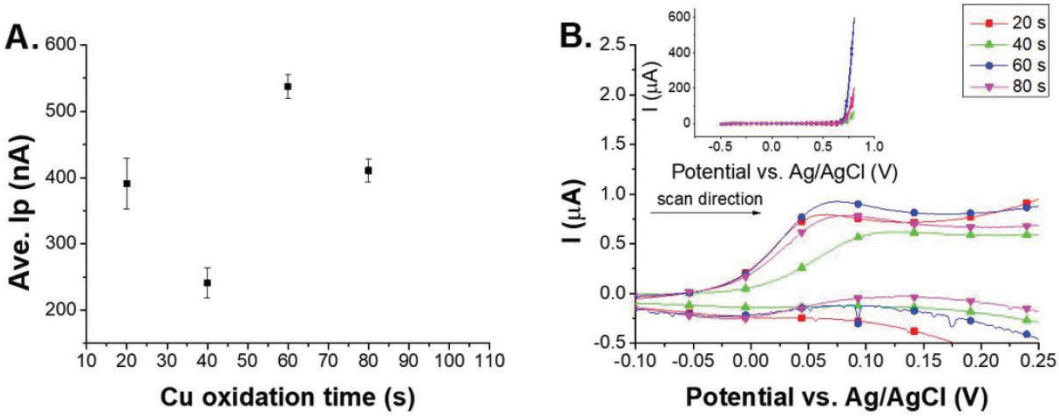

Figure IV. (A) Optimization graph for the optimization of Cu oxidation time. (B) CV curves of 20 μM H_2O_2 in 0.1 M NaOH using CuO-CPEs (Cu deposition time: 40 s, equilibration time: 40 s) with different Cu oxidation times; scan rate: 10 mV/s. The inset shows the whole CV curves.

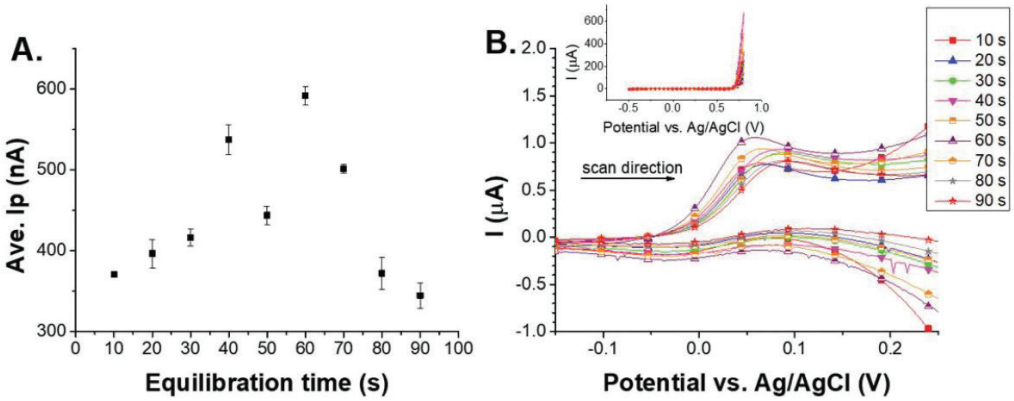

Figure V. (A) Optimization graph for the optimization of equilibration time. (B) CV curves of 20 μM H_2O_2 in 0.1 M NaOH using CuO-CPEs (Cu deposition time: 40 s, Cu oxidation time: 60 s) with different equilibration times; scan rate: 10 mV/s. The inset shows the whole CV curves.

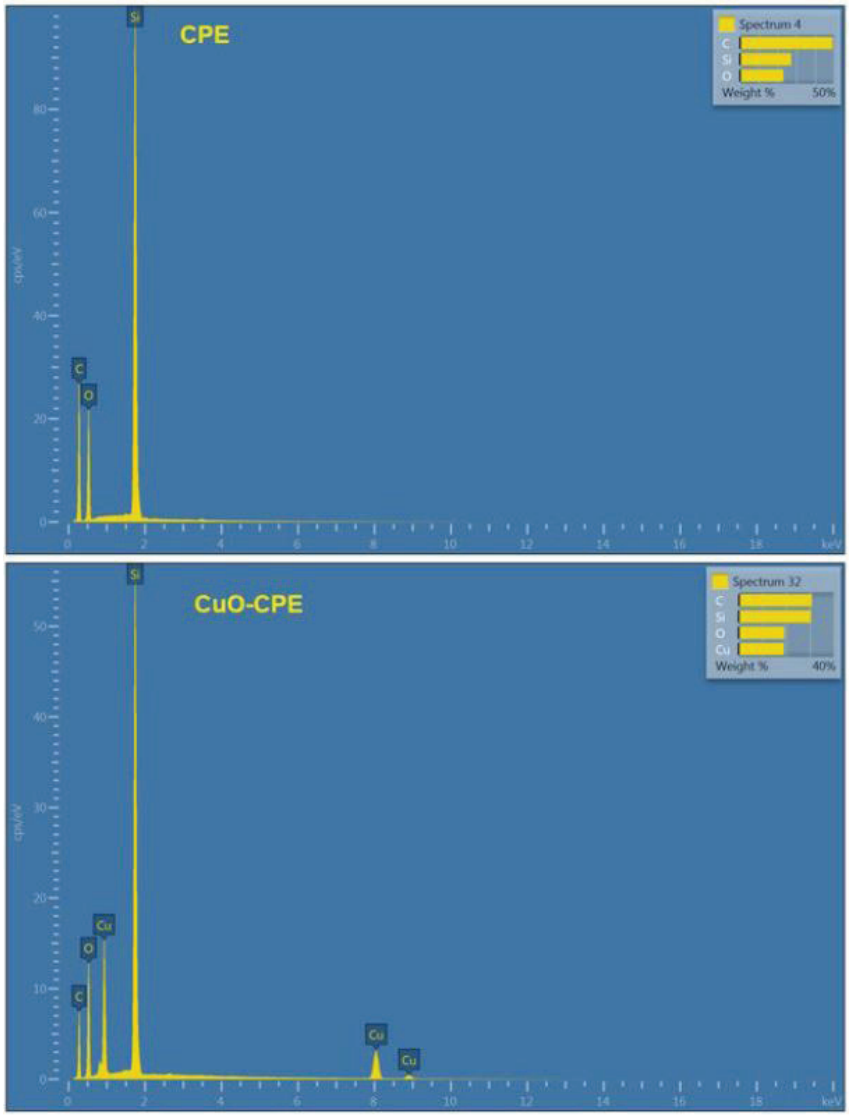

Figure VI. EDX spectrum for (A) CPE and (B) CuO-CPE.

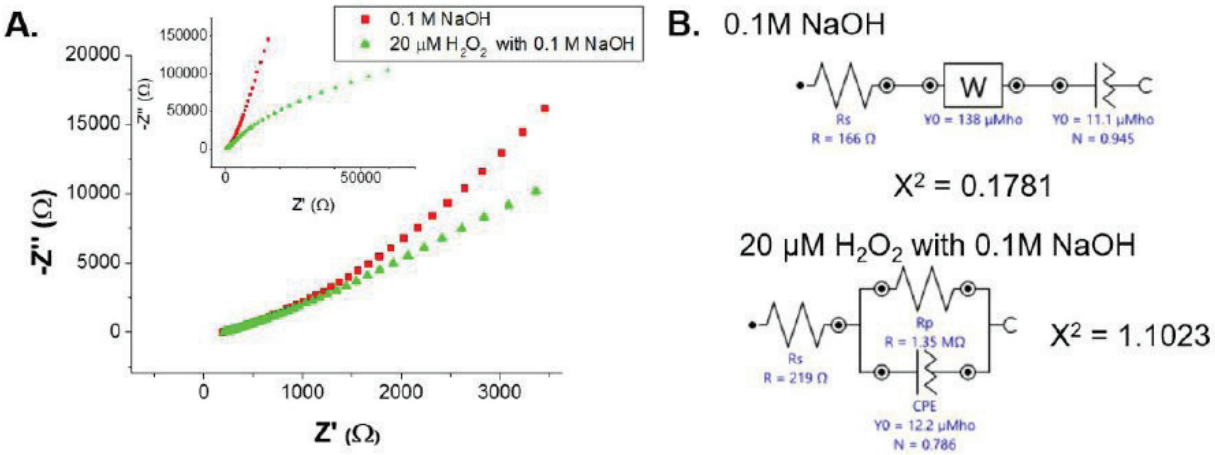

Figure VII. (A) Nyquist plots from EIS measurements using CuO-CPE under different solutions. (B) Fitted equivalent circuit models from EIS measurements. CuO-CPE in different solutions. Frequency used: 0.1 Hz to 20 kHz; applied potential: 0.07 V. Chi-squared values (x^2) were indicated for evaluation of curve fitting.